POLITECNICO DI TORINO
Repository ISTITUZIONALE

Cathode-Electrolyte Interphase in a LiTFSI/Tetraglyme Electrolyte Promoting the Cyclability of V2O5

(Article begins on next page)

26 December 2024

Cathode-Electrolyte Interphase in LiTFSI:Tetraglyme Electrolyte Promoting Cyclability of V_2O_5

Xu Liu,[a,b] Maider Zarrabeitia,[a,b] Bingsheng Qin,[a,b] Giuseppe Antonio Elia,[a,b]* Stefano Passerini[a,b]*

[a]Helmholtz Institute Ulm (HIU) Electrochemical Energy Storage, Helmholtzstrasse 11, 89081, Germany

[b] Karlsruhe Institute of Technology (KIT), PO Box 3640, D-76021 Karlsruhe, Germany

ABSTRACT

V_2O_5, one of the earliest intercalation-type cathode materials investigated as Li^+ host, is characterized by an extremely high theoretical capacity (441 mAh g^{-1}). However, the fast capacity fading upon cycling in conventional carbonate-based electrolytes is an unresolved issue. Herein, we show that using the LiTFSI:Tetraglyme (1:1 in mole ratio) electrolyte yields to a highly enhanced cycling ability of V_2O_5 (from 20% capacity retention to 80% after 100 cycles at 50 mA g^{-1} within 1.5 - 4.0 V $vs.$ Li^+/Li). The improved performance mostly originates from the V_2O_5 electrode itself since refreshing the electrolyte and lithium electrode of the cycled cells does not help in restoring the V_2O_5 electrode capacity. Electrochemical impedance spectroscopy (EIS), post-mortem scanning electron microscopy (SEM), energy-dispersive X-ray (EDX) spectroscopy, and X-ray photoelectron spectroscopy (XPS) have been employed to investigate the origin of the improved electrochemical behavior. The results demonstrate that the enhanced cyclability is a consequence of a thinner, but more stable cathode-electrolyte interphase (CEI) layer formed in LiTFSI:Tetraglyme with respect to the one occurring in 1 M $LiPF_6$ in EC:DMC (1:1 in weight ratio, LP30). These results show that the cyclability of V_2O_5 can be effectively improved by simple electrolyte engineering. At the same time, the uncovered mechanism further reveals the vital role of CEI on the cyclability of V_2O_5, which can be helpful for the performance optimization of vanadium oxide-based batteries.

KEYWORDS: Lithium batteries, Highly concentrated electrolytes, Cathode-electrolyte interphase, Tetraglyme, Vanadium oxides

INTRODUCTION

The limited supply of critical materials, *e.g.*, lithium, nickel, and particularly cobalt, for the state-of-the-art lithium-ion batteries, is pushing the research efforts toward alternative batteries relying on more abundant metal cation carriers,[1] *e.g.*, Na$^+$,[2–5] K$^+$,[6,7] Mg^{2+},[8] Ca^{2+},[9] Zn^{2+},[10] and Al^{3+}.[11] However, their higher charge density and/or larger ionic radius compared with Li$^+$ lead to difficulties in finding suitable cathode host materials, especially for multivalent batteries.[8,9,12] Among the limited choices, vanadium oxide-based materials are promising candidates.[13] Their tunable crystal structure usually offers large tunnels or interlayer space for the intercalation of the above-mentioned cation guests,[14] while the multielectron transition of the metal (V$^{3+/5+}$) provides high theoretical specific capacities.[15] Therefore, these materials have been widely investigated as hosts for various battery chemistries employing the above-mentioned cations.[16–21] However, the high specific capacity and good rate performance in these batteries are usually accompanied by fast capacity fading, especially at low rates, which limits the practical use of vanadium oxides.[22–26] Searching for feasible strategies to enhance the cyclability of vanadium oxides and further explore the mechanism behind could lead to vanadium oxide-based batteries with optimized performance. Due to the complexity of the newly emerging cell chemistries, whose components have not been well investigated, we selected a mature battery technology, *i.e.*, lithium-based batteries, to reduce the complexity in the investigation of the fading mechanism.

Orthorhombic V$_2$O$_5$ is one of the earliest materials explored as reversible hosts for Li$^+$, which can be traced back to more than 40 years ago.[27] V$_2$O$_5$ exhibits an extremely high theoretical capacity (441 mAh g^{-1}, 1.5-4.0 V *vs*. Li$^+$/Li), thus attracting broad research interests in the early exploration of cathode host materials for Li$^+$.[28] Its structural evolution and electrochemical behavior upon (de-)lithiation have been well investigated and presented.[29] However, the severe

capacity fading is still an unsolved issue. Therefore, Li/orthorhombic V_2O_5 battery is an excellent model to investigate the parameters affecting the cyclability of vanadium oxide-based materials. Several approaches have been applied to mitigate the fast capacity fading of V_2O_5, including the addition of secondary components,[30] lattice dopant,[31] and nano-architectures.[22] Nonetheless, a capacity fading of 0.5-2.5% per cycle within the operation window of 1.5-4.0 V *vs*. Li^+/Li is still commonly seen in the literature.[22] Therefore, strategies focusing only on the electrode materials are not enough to resolve the reduced lifespan of V_2O_5. Other cell components playing an active role in the cell need to be considered, such as the electrolyte.

Herein, we underline the importance of the proper electrolyte design to tune the battery performance at a higher level. The reported results indicate that the replacement of LP30 carbonate electrolyte with LiTFSI:Tetraglyme electrolyte (mole ratio 1:1) leads to enhanced cyclability of V_2O_5. Through refreshing the electrolyte and lithium electrode of the cycled cells, to eliminate the effect originating from the anode degradation, it is proved that the enhanced cycling ability mainly originates from the cathode side. SEM, EDX, X-ray diffraction (XRD), XPS, and EIS were carried out to investigate further the mechanism responsible for the improved capacity retention.

RESULTS AND DISCUSSION

The crystal structure of commercial orthorhombic V_2O_5, herein used as the model material, was investigated *via* XRD (Figure S1). The SEM image (Figure S1b) shows that the V_2O_5 powder is composed of large aggregates (50-60 µm) formed by smaller particles with dimensions ranging in the 0.5-2 µm.

The cyclability of the V_2O_5 electrodes was investigated in three-electrode cells, employing lithium reference and counter electrodes, at low specific current (50 mA g^{-1}) to reduce the influence of the lithium negative electrode. The first cycle voltage profiles of V_2O_5 electrodes in the two

electrolytes, and their derivative curves are reported in Figure 1a and b, respectively. The observed voltage plateaus and differential peaks are associated with the α→ε and ε→δ phase transitions in the 3.4-2.7 V region (peak 1), which are followed by the δ→γ phase transition occurring in the 2.5-2.0 V region (peak 2) and the γ→ω phase transition taking place in the 2.0-1.5 V region (peak 3).[32] The last phase transition is irreversible. In fact the following reversible cycling involves only the transition between the disordered ω- and β- phases.[32,33] However, the voltage plateaus (Figure 1c and e) and differential capacity peaks (Figure 1d and f) related to the phase transitions are observed until the 5th cycle, demonstrating that the irreversible transition from initial α- to ω-phase is not complete after the first discharge. In both electrolytes, the complete transformation to the ω phase occurs only after the 5th cycle as demonstrated by the typical sloping voltage profile of disordered V_2O_5.

Figure 2a shows the evolution of discharge specific capacity comparison upon 100 charge-discharge cycles for the Li/V_2O_5 cells employing the LP30 and the LiTFSI:Tetraglyme electrolytes. For both systems, the irreversibility in the initial cycles is mainly due to the irreversible transition from α- to ω-phases. Upon further cycling, the higher viscosity and lower ionic conductivity of the LiTFSI:Tetraglyme electrolyte[34] leads to lower initial capacity, however, with an improved cyclability. The capacity slowly decreases from 266 mAh g^{-1} at the 6th cycle to 225 mAh g^{-1} at the 100th cycle, exhibiting a capacity retention of 84%. With the conventional carbonate electrolyte (LP30), the capacity rapidly decreases from 309 mAh g^{-1} at the 6th cycle to 63 mAh g^{-1} at the 100th cycle, retaining only 20% of the initial capacity. Similar phenomena are also observed at elevated specific current, i.e., 440 mA g^{-1}, as shown in Figure S2. These results demonstrate that the use of the highly concentrated LiTFSI:Tetraglyme electrolyte can effectively promote the cyclability of V_2O_5 as a reversible cathode host material for Li$^+$.

Figure 2b displays the Coulombic efficiency (CE, calculated as $Q_{discharge}/Q_{charge}$) evolution upon cycling. The observed CE values higher than 100% in the initial cycles relate to the irreversible phase transitions occurring in the electrode material, which result in Li trapping. In fact, the CE value for the cell employing the LiTFSI:Tetraglyme electrolyte reaches a stable value (about 99.98%) after 15 cycles, indicating for the high reversibility of the (de-)lithiation process. However, in LP30 electrolyte, the steady-state CE is always higher than 100% (~103%), which implies continuous side reactions during the reduction (discharge) process upon cycling, e.g., electrolyte decomposition[35] or/and vanadium oxide dissolution[36]. To evaluate the origin of the capacity decay, the cycled V_2O_5 electrodes were unmounted from the cells after 100 cycles and coupled with fresh lithium electrodes and electrolytes.[37] The charge-discharge profiles at 50 mA g^{-1} of the reassembled cells are displayed in Figure 2c. These tests reveal that no capacity recovery is observed for the electrodes tested with both LP30 and LiTFSI:Tetraglyme electrolytes, suggesting that the observed capacity fading originates mostly from the cathode side rather than degradation of the lithium electrode or the electrolyte. The possible influence in the intercalation process of the electrolyte was verified by ex-situ XRD of the cycled electrodes at their de-lithiated state (Figure S2). However, after 100 cycles, the XRD patterns of the electrodes cycled in the two electrolytes are very similar. Because the anion and solvent are not involved in the intercalation in disordered V_2O_5, these two electrolytes unlikely affect the Li$^+$ intercalation/de-intercalation mechanism in V_2O_5. Therefore, it is reasonable to infer that the capacity decay does not result from the structural instability of V_2O_5 or degradation of lithium metal electrodes.

Figure 3 shows selected charge-discharge profiles and the resulting derivative capacity profiles of the Li/V_2O_5 cells upon cycling test performed using LP30 (Figure 3a and c) and LiTFSI:Tetraglyme (Figure 3b and d) electrolytes at 50 mA g^{-1}. The fast fading observed in LP30

electrolyte exhibits dramatic changes in the potential profiles upon cycling (Figure 3a), clearly recognized in the differential capacity profiles (Figure 3c). The decreased peak intensity, associated with the capacity fading, is also accompanied by an increase in cell polarization as indicated by the shift of the peaks positions. In contrast, the use of LiTFSI:Tetraglyme only leads to minor changes of both the peak potential and intensity in the differential capacity plots of the cell upon 100 cycles (Figures 3b and d), which is in agreement with the excellent capacity retention observed above.

Figures 4a-c display the SEM images of pristine and cycled V_2O_5 electrodes. In the pristine electrode (Figure 4a), the submicron V_2O_5 particles exhibit a smooth surface. After 100 cycles, the particle shape does not change for both electrolytes. Considering the severe capacity fading in LP30 electrolyte (capacity retention is only 20% after 100 cycles), one can conclude that the dissolution of vanadium oxide reported in previous literatures is not the main reason for the capacity fading.[36,38] Meanwhile, it is observed that the particles cycled in LP30 appear much rougher and coated by a net-like deposit (Figure 4b) which is not observed on the surface of V_2O_5 cycled in the LiTFSI:Tetraglyme electrolyte (Figure 4c). The EDX spectra displayed in Figure 4d evidence that the electrode cycled in LP30 exhibits higher content of C and F, compared with both the pristine electrode and the one cycled in LiTFSI:Tetraglyme. This suggests different chemistries of the formed CEI in the different electrolyte formulation.

XPS experiments were carried on the cycled electrodes (after 100 cycles) in the two electrolytes to further investigate their surface chemistries. The intensity scale was included and kept the same in both systems (except for O 1s surface spectrum of the electrode tested in LP30 because it shows a much higher carbonate signal). Figure 5 a and b display the F 1s and O 1s + V 2p regions, respectively, of the electrode tested in LP30. The low intensity of V 2p peak and the presence of

several species with -C-O- and -F bonds in the O 1s and F 1s regions, respectively, clearly indicate that a CEI covers the V_2O_5 particle surface after cycling.[39] The O 1s spectrum of the surface demonstrates that a Li_2CO_3-rich layer covers the electrode tested in LP30 (note that the carbonate signal is the main component). At higher depth (~4.8 nm), the carbonate signal decreases, revealing a chemically different layer characterized by a lower amount of Li_2CO_3, but an increase of $LiCO_3R$ (R = alkyl chain), $Li_xPO_yF_z$, LiF and other species with –COC- groups. Interestingly, a third layer is observed close to the electrode (~9.6 nm in-depth), mainly consisting of –COC- species, and $Li_xPO_yF_z$ (shown in the schematic of the CEI, Figure 5c). Therefore, the CEI formed on the V_2O_5 cycled in LP30 shows three chemically different layers: an organic-rich layer close to the electrode and an inorganic-rich layer close to the electrolyte, separated by a mixed organic/inorganic layer in-between.

Figures 5c and d display the F1s and O 1s + V 2p XPS spectra of the electrode cycled in the LiTFSI:Tetraglyme, respectively. Comparing the F 1s and O 1s regions with those obtained in the LP30, one can find that despite the similarity on the formed species, the CEI formed in LiTFSI:Tetraglyme is not carbonate-rich as in LP30 electrode. In fact, a LiTFSI-rich layer mixed with –COC- species and a lower amount of Li_2CO_3, $LiCO_3R$, and LiF is formed. At higher depths, i.e., ~4.8 and ~9.6 nm, the CEI is composed mainly of LiF. No change of composition is observed at these depths, in contrast with the multilayer structure of the CEI observed in LP30 electrode (compare Figure 5 c and f). In addition, it is known that LiF is a good electric insulator and can effectively block electron leakage through the interface, further mitigating the electrolyte decomposition upon cycling and resulting in a better CE.[40]

These results demonstrate that the CEI formed in LiTFSI:Tetraglyme possesses a low amount of carbonate-based species, but more -COC- species. Additionally, more LiF is formed in this

electrolyte than in LP30 where more Li_xPF_y or $Li_zPO_yF_z$ are formed. These differences can be reasonably attributed to the different salt, solvent, salt concentration and, consequently, different solvation in LP30 and LiTFSI:Tetraglyme electrolytes, implying that the V_2O_5/electrolyte interphase can be effectively tuned via the electrolyte formulation.

Besides the difference in chemical composition, the CEI formed in LP30 is evidently thicker than that in LiTFSI:Tetraglyme. Comparing the O 1s spectra for the two electrodes at different depths, one can find that the V-O related peak is much smaller for LP30. Meanwhile, the relative intensity of V 2p against O 1s on the surface spectrum is much lower for LP30 than for LiTFSI:Tetraglyme. Furthermore, the peak located at 284.4 eV on C 1s (Figure S3), which results from -C-C- sp^2 bonding and mainly corresponds to the conductive additive (C65),[41] shows a lower intensity in LP30, again suggesting that the CEI is thicker for the electrode tested in LP30.

The difference in the CEI thickness and chemical composition of the electrodes cycled in LP30 and LiTFSI:Tetraglyme agrees well with the electrochemical results reported in Figures 2-3 and the different deposit morphologies shown in the SEM images (Figure 4). The reported SEM, EDX, and the XPS results present the composition and morphology of the CEI accumulated upon 100 charge-discharge cycles. These results indicate that the net-like deposits formed on V_2O_5 cycled in LP30 (Figure 4b) are mainly composed of lithium carbonate and lithium fluorophosphates.

To get a better understanding of the effect of the different CEI compositions on the electrochemical behavior, EIS was carried out.[SP1][XL2] The Nyquist plots of the V_2O_5 electrode in the initial 10 cycles in LP30 and LiTFSI:Tetraglyme are shown in Figures 6a and b, respectively. The EIS data can be well fitted according to the equivalent circuit shown in Figure 6c. Aurbach *et al*. have insightfully investigated the EIS of V_2O_5 material and assigned the elements to specific electrochemical processes.[42] The high-frequency intercept (Z_{Re}) corresponds to a pure resistor (R1)

associated with the bulk resistance of the electrolyte and electrodes. Three depressed semicircles (R2//Q2, R3//Q3, R4//Q4) can be observed at lower frequencies. R2//Q2 and R3//Q3 stand for the Li^+ migration through the surface layer covering the V_2O_5, while R4//Q4 relates to the Li^+ transfer across the surface layer/V_2O_5 interface.[42] At very low frequency, the diffusion limitation in the bulk of the electrode occurs, noted as a Warburg element. The variation R1 (Figure R1) relates to variation in the electrolyte resistance, while R2+R3+R4, summarized in Figure 6d, reflects the influence of CEI in the electrochemical process. The R1 value is higher for the Tetraglyme-based electrolyte, due to its lower ionic conductivity.[34] For both electrolytes, the R1 values are stable upon the reported 10 cycles, suggesting no massive degradation of the electrolyte.

In contrast, the value of (R2+R3+R4) shows a different behavior in the two electrolytes. After a small increase in the initial four cycles, this resistance value is seen to decrease for the electrode tested in LiTFSI:Tetraglyme. On the other hand, it continuously increases upon cycling in LP30. Thus, despite the lower initial value, (R2+R3+R4) in LP30 electrolyte becomes higher than in LiTFSI:Tetraglyme after only six cycles. With more cycles in the LP30 electrolyte, the V_2O_5 electrode exhibits a significant increase of the impedance (Figure S5(a)), and the cell cannot operate after 60 cycles. While the V_2O_5 electrode cycled in the LiTFSI:Tetragyme electrolyte still maintains a low impedance even after 100 cycles (Figure S5(b)). The results are also in good agreement with the CE upon cycling (Fig. 2b), SEM images (Fig. 4), and XPS analysis (Fig. 5). Overall, it is reasonable to conclude that the poor cyclability of V_2O_5 in LP30 electrolyte is a consequence of the unstable and more resistive CEI hindering the Li^+ migration and transfer.

CONCLUSION

The rapid capacity fading of V_2O_5 upon cycling in conventional, carbonate-based electrolytes can be effectively mitigated *via* employing the LiTFSI:Tetraglyme electrolyte. The enhanced

cyclability mainly originates from a more stable and thinner CEI, mainly composed of LiF and organic ether species (-COC-) in the innermost layer and an outermost layer composed of LiTFSI and –COC-, resulting from the specific solvent, salt and its concentration, and, consequently, different solvation. The obtained results indicate that the cyclability of V_2O_5 can be improved by electrolyte engineering, while the uncovered mechanism further reveals the vital role of CEI on the cyclability of V_2O_5. The insight on the CEI characteristics gives fundamental information, essential for the performance optimization of vanadium oxide-based batteries.

EXPERIMENTAL SECTION

Materials

V_2O_5 (Pechiney), *N*-Methyl-2-pyrrolidone (NMP, anhydrous, Sigma Aldrich), Polyvinylidene fluoride (PVdF, Solef 6020), carbon black (Super C65, Imerys), glass fiber sheet (Whatman GF/F), LP30 (BASF, battery grade), lithium metal (Honjo, battery grade), and dimethyl carbonate (DMC, UBE, battery grade) were directly used as received. Molecular sieves (3 Å, Alfa Aesar) were dried at 300 °C under vacuum (10^{-3} mbar) for more than one week. LiTFSI (3M Co., Ltd.) was dried at 120 °C under vacuum (10^{-3} mbar) for 12 h before use. The residual water in tetraethylene glycol dimethyl ether (tetraglyme, Sigma-Aldrich, 99%) was removed *via* the dried molecular sieves before use.

Physical-chemical characterization

XRD was conducted on a diffractometer (D8 Advance Bruker, Germany) equipped with Cu-$K\alpha_{1,2}$ = 1.5418 Å) radiation. SEM images of the as-prepared sample were obtained using a Zeiss LEO 1550 microscope equipped with EDX spectroscopy (Oxford Instruments X-MaxN, 50 mm^2, 15 kV). XPS measurements were conducted in an ultrahigh vacuum surface analysis system (10^{-10} mbar) by Phoibos 150 XPS spectrometer (SPECS –Surface concept) equipped with a micro-

channel plate and Delay Line Detector and monochromatized Al Kα (1486.6 eV) X-ray. The depth profiling was carried out using a focused ion gun for 5 keV Ar$^+$, for 6 and 12 mins. The peak fitting was carried out by CasaXPS software, using Shiley-type background and 70% Gaussian – 30% Lorentzian profile function. For the post-mortem characterization, the electrodes were removed from Swagelok-type T-cells in an Ar-filled glove box with H_2O and O_2 levels < 0.1 ppm (MBraun). The samples were sealed in a plastic vessel to prevent exposure to humid air for XRD measurements, and for SEM, EDS, and XPS measurements, sealed in transfer boxes.

Electrochemical measurements

The electrodes were fabricated by doctor-blade casting of slurries with 70 wt% V_2O_5, 20 wt.% Super C65, and 10 wt% PVdF binder on aluminum foil (current collector). NMP was used as the solvent. After the solvent is evaporated with an electronic oven at 60 °C, electrodes with a diameter of 12 mm were punched and further dried at 120 °C under vacuum (1×10^{-3} mbar) for 12 h. The average mass loading of the active material was around 2 mg cm^{-2}. The electrolyte preparation and cell assembly were carried out in an Ar-filled glove box with H_2O and O_2 levels < 0.1 ppm (MBraun). The LiTFSI:Tetraglyme electrolyte was prepared by dissolving equal mole LiTFSI in tetraglyme. To evaluate the electrochemical behaviors of the V_2O_5 electrodes in LP30 and LiTFSI:Tetraglyme, three-electrode Swagelok type T cells employing lithium metal as counter and reference electrodes, and GF/F disks as separators were assembled. In each cell, 120 µL electrolytes were used. Cycling ability was tested at 50 mA g^{-1}, 20°C temperature *via* the MACCOR Series 4000 Battery Cycler. The EIS were conducted using the galvanostat/potentiostat VMP3 (Bio-Logic, France) and analyzed with Boukamp software.[43]

ASSOCIATED CONTENT

Supporting Information. XRD and SEM images of the V_2O_5 particles; XRD pattern of carbon black, the pristine V_2O_5 electrode, and the ones after 100 cycles in different electrolytes; C 1s XPS of cycled V_2O_5 electrodes.

AUTHOR INFORMATION

Corresponding Author

E-mail: giuseppe.elia@kit.edu; stefano.passerini@kit.edu

Notes

Any additional relevant notes should be placed here.

REFERENCES

(1)   Vaalma, C.; Buchholz, D.; Weil, M.; Passerini, S. A Cost and Resource Analysis of Sodium-Ion Batteries. *Nat. Rev. Mater.* **2018**, *3* (4), 18013. https://doi.org/10.1038/natrevmats.2018.13.

(2)   Eshetu, G. G.; Elia, G. A.; Armand, M.; Forsyth, M.; Komaba, S.; Rojo, T.; Passerini, S. Electrolytes and Interphases in Sodium-Based Rechargeable Batteries: Recent Advances and Perspectives. *Adv. Energy Mater.* **2020**, 2000093.

https://doi.org/10.1002/aenm.202000093.

(3)   Xu, J.; Gu, E.; Zhang, Z.; Xu, Z.; Xu, Y.; Du, Y.; Zhu, X.; Zhou, X. Fabrication of Porous

Na3V2(PO4)3/Reduced Graphene Oxide Hollow Spheres with Enhanced Sodium Storage

Performance.   *J.   Colloid   Interface   Sci.*   **2020**,   *567*,   84–91.

https://doi.org/10.1016/j.jcis.2020.01.121.

(4)   Zhang, Z.; Du, Y.; Wang, Q. C.; Xu, J.; Zhou, Y. N.; Bao, J.; Shen, J.; Zhou, X. A Yolk–

Shell-Structured FePO4 Cathode for High-Rate and Long-Cycling Sodium-Ion Batteries.

Angew.   Chemie   -   Int.   Ed.   **2020**,   *59*   (40),   17504–17510.

https://doi.org/10.1002/anie.202008318.

(5)   Zhongfan, L. Insight into Effects of Fluoroethylene Carbonate Additive on the Cathode in

Sodium Ion Batteries. *Wuli Huaxue Xuebao/ Acta Phys. - Chim. Sin.* **2019**, *35* (8), 804–805.

https://doi.org/10.3866/PKU.WHXB201903013.

(6)   Pramudita, J. C.; Sehrawat, D.; Goonetilleke, D.; Sharma, N. An Initial Review of the Status

of Electrode Materials for Potassium-Ion Batteries. *Advanced Energy Materials*. 2017.

https://doi.org/10.1002/aenm.201602911.

(7)   Ge, X.; Liu, S.; Qiao, M.; Du, Y.; Li, Y.; Bao, J.; Zhou, X. Enabling Superior

Electrochemical Properties for Highly Efficient Potassium Storage by Impregnating

Ultrafine Sb Nanocrystals within Nanochannel-Containing Carbon Nanofibers. *Angew.

Chemie* **2019**, *131* (41), 14720–14725. https://doi.org/10.1002/ange.201908918.

(8)   Canepa, P.; Sai Gautam, G.; Hannah, D. C.; Malik, R.; Liu, M.; Gallagher, K. G.; Persson,

K. A.; Ceder, G. Odyssey of Multivalent Cathode Materials: Open Questions and Future

Challenges. *Chem. Rev.* **2017**, *117* (5), 4287–4341. https://doi.org/10.1021/acs.chemrev.6b00614.

(9)   Dugas, R.; Forero-Saboya, J. D.; Ponrouch, A. Methods and Protocols for Reliable Electrochemical Testing in Post-Li Batteries (Na, K, Mg, and Ca). *Chem. Mater.* **2019**. https://doi.org/10.1021/acs.chemmater.9b02776.

(10)   Fang, G.; Zhou, J.; Pan, A.; Liang, S. Recent Advances in Aqueous Zinc-Ion Batteries. *ACS Energy Lett.* **2018**, *3* (10), 2480–2501. https://doi.org/10.1021/acsenergylett.8b01426.

(11)   Elia, G. A.; Marquardt, K.; Hoeppner, K.; Fantini, S.; Lin, R.; Knipping, E.; Peters, W.; Drillet, J.-F.; Passerini, S.; Hahn, R. An Overview and Future Perspectives of Aluminum Batteries. *Adv. Mater.* **2016**, *28* (35), 7564–7579. https://doi.org/10.1002/adma.201601357.

(12)   Tang, B.; Shan, L.; Liang, S.; Zhou, J. Issues and Opportunities Facing Aqueous Zinc-Ion Batteries. *Energy Environ. Sci.* **2019**, *12* (11), 3288–3304. https://doi.org/10.1039/c9ee02526j.

(13)   Xu, X.; Xiong, F.; Meng, J.; An, Q.; Mai, L. Multi-Electron Reactions of Vanadium-Based Nanomaterials for High-Capacity Lithium Batteries: Challenges and Opportunities. *Mater. Today Nano* **2020**. https://doi.org/10.1016/j.mtnano.2020.100073.

(14)   Song, M.; Tan, H.; Chao, D.; Fan, H. J. Recent Advances in Zn-Ion Batteries. *Adv. Funct. Mater.* **2018**, *28* (41), 1–27. https://doi.org/10.1002/adfm.201802564.

(15)   Moretti, A.; Maroni, F.; Nobili, F.; Passerini, S. V2O5 Electrodes with Extended Cycling Ability and Improved Rate Performance Using Polyacrylic Acid as Binder. *Journal of Power Sources*. 2014, pp 1068–1072. https://doi.org/10.1016/j.jpowsour.2014.09.150.

(16) Moretti, A.; Passerini, S. Bilayered Nanostructured V2O5·nH2O for Metal Batteries. *Advanced Energy Materials*. 2016. https://doi.org/10.1002/aenm.201600868.

(17) Liu, X.; Qin, B.; Zhang, H.; Moretti, A.; Passerini, S. Glyme-Based Electrolyte for Na/Bilayered-V 2 O 5 Batteries. *ACS Appl. Energy Mater.* **2019**, *2* (4), 2786–2793. https://doi.org/10.1021/acsaem.9b00128.

(18) Liu, X.; Zhang, H.; Geiger, D.; Han, J.; Varzi, A.; Kaiser, U.; Moretti, A.; Passerini, S. Calcium Vanadate Sub-Microfibers as Highly Reversible Host Cathode Material for Aqueous Zinc-Ion Batteries. *Chem. Commun.* **2019**, *55* (16), 2265–2268. https://doi.org/10.1039/c8cc07243d.

(19) Liu, X.; Elia, G. A.; Gao, X.; Qin, B.; Zhang, H.; Passerini, S. Highly Concentrated KTFSI : Glyme Electrolytes for K/Bilayered-V 2 O 5 Batteries . *Batter. Supercaps* **2020**, 1–8. https://doi.org/10.1002/batt.202000003.

(20) Wan, F.; Zhang, L.; Dai, X.; Wang, X.; Niu, Z.; Chen, J. Aqueous Rechargeable Zinc/Sodium Vanadate Batteries with Enhanced Performance from Simultaneous Insertion of Dual Carriers. *Nat. Commun.* **2018**, *9* (1), 1–11. https://doi.org/10.1038/s41467-018-04060-8.

(21) Xu, X.; Duan, M.; Yue, Y.; Li, Q.; Zhang, X.; Wu, L.; Wu, P.; Song, B.; Mai, L. Bilayered Mg0.25V2O5·H2O as a Stable Cathode for Rechargeable Ca-Ion Batteries. *ACS Energy Lett.* **2019**. https://doi.org/10.1021/acsenergylett.9b00830.

(22) Yue, Y.; Liang, H. Micro- and Nano-Structured Vanadium Pentoxide (V2O5) for Electrodes of Lithium-Ion Batteries. *Advanced Energy Materials*. 2017.

https://doi.org/10.1002/aenm.201602545.

(23)   Wei, Q.; Liu, J.; Feng, W.; Sheng, J.; Tian, X.; He, L.; An, Q.; Mai, L. Hydrated Vanadium

Pentoxide with Superior Sodium Storage Capacity. *J. Mater. Chem. A* **2015**.

https://doi.org/10.1039/c5ta00502g.

(24)   Clites, M.; Hart, J. L.; Taheri, M. L.; Pomerantseva, E. Chemically Preintercalated

Bilayered KxV2O5· n H2O Nanobelts as a High-Performing Cathode Material for K-Ion

Batteries.   *ACS   Energy   Lett.*   **2018**,   *3*   (3),   562–567.

https://doi.org/10.1021/acsenergylett.7b01278.

(25)   Gao, X.; Mariani, A.; Jeong, S.; Liu, X.; Dou, X.; Ding, M.; Moretti, A.; Passerini, S.

Prototype Rechargeable Magnesium Batteries Using Ionic Liquid Electrolytes. *J. Power*

Sources **2019**, *423* (March), 52–59. https://doi.org/10.1016/j.jpowsour.2019.03.049.

(26)   Yang, Y.; Tang, Y.; Fang, G.; Shan, L.; Guo, J.; Zhang, W.; Wang, C.; Wang, L.; Zhou, J.;

Liang, S. Li+ Intercalated V2O5·: N H2O with Enlarged Layer Spacing and Fast Ion

Diffusion as an Aqueous Zinc-Ion Battery Cathode. *Energy Environ. Sci.* **2018**.

https://doi.org/10.1039/c8ee01651h.

(27)   Whittingham, M. S. The Role of Ternary Phases in Cathode Reactions. *J. Electrochem. Soc.*

1976. https://doi.org/10.1149/1.2132817.

(28)   Yao, J.; Li, Y.; Massé, R. C.; Uchaker, E.; Cao, G. Revitalized Interest in Vanadium

Pentoxide as Cathode Material for Lithium-Ion Batteries and Beyond. *Energy Storage*

Materials. 2018. https://doi.org/10.1016/j.ensm.2017.10.014.

(29)   Baddour-Hadjean, R.; Marzouk, A.; Pereira-Ramos, J. P. Structural Modifications of

LixV2O5 in a Composite Cathode (0≤x < 2) Investigated by Raman Microspectrometry. *J. Raman Spectrosc.* **2012**, *43* (1), 153–160. https://doi.org/10.1002/jrs.2984.

(30) Cheng, J.; Wang, B.; Xin, H. L.; Yang, G.; Cai, H.; Nie, F.; Huang, H. Self-Assembled V2O5 Nanosheets/Reduced Graphene Oxide Hierarchical Nanocomposite as a High-Performance Cathode Material for Lithium Ion Batteries. *J. Mater. Chem. A* **2013**. https://doi.org/10.1039/c3ta12066j.

(31) Song, H.; Liu, C.; Zhang, C.; Cao, G. Self-Doped V4+-V2O5 Nanoflake for 2 Li-Ion Intercalation with Enhanced Rate and Cycling Performance. *Nano Energy* **2016**. https://doi.org/10.1016/j.nanoen.2016.02.004.

(32) Christensen, C. K.; Sørensen, D. R.; Hvam, J.; Ravnsbæk, D. B. Structural Evolution of Disordered Li x V 2 O 5 Bronzes in V 2 O 5 Cathodes for Li-Ion Batteries. *Chem. Mater.* **2019**. https://doi.org/10.1021/acs.chemmater.8b04558.

(33) Feng, C. Q.; Wang, S. Y.; Zeng, R.; Guo, Z. P.; Konstantinov, K.; Liu, H. K. Synthesis of Spherical Porous Vanadium Pentoxide and Its Electrochemical Properties. *J. Power Sources* **2008**, *184* (2), 485–488. https://doi.org/10.1016/j.jpowsour.2008.04.049.

(34) Dokko, K.; Tachikawa, N.; Yamauchi, K.; Tsuchiya, M.; Yamazaki, A.; Takashima, E.; Park, J.-W.; Ueno, K.; Seki, S.; Serizawa, N.; Watanabe, M. Solvate Ionic Liquid Electrolyte for Li–S Batteries. *J. Electrochem. Soc.* **2013**. https://doi.org/10.1149/2.111308jes.

(35) Fleutot, B.; Martinez, H.; Pecquenard, B.; Ledeuil, J. B.; Levasseur, A.; Gonbeau, D. Surface Film Morphology (AFM) and Chemical Features (XPS) of Cycled V2O5 Thin

Films in Lithium Microbatteries. *J. Power Sources* **2008**, *180* (2), 836–844. https://doi.org/10.1016/j.jpowsour.2008.02.080.

(36) Moretti, A.; Jeong, S.; Passerini, S. Enhanced Cycling Ability of V2O5 Aerogel Using Room-Temperature Ionic Liquid-Based Electrolytes. *ChemElectroChem* **2016**, *3* (7), 1048–1053. https://doi.org/10.1002/celc.201600040.

(37) Jiao, S.; Ren, X.; Cao, R.; Engelhard, M. H.; Liu, Y.; Hu, D.; Mei, D.; Zheng, J.; Zhao, W.; Li, Q.; Liu, N.; Adams, B. D.; Ma, C.; Liu, J.; Zhang, J. G.; Xu, W. Stable Cycling of High-Voltage Lithium Metal Batteries in Ether Electrolytes. *Nat. Energy* **2018**. https://doi.org/10.1038/s41560-018-0199-8.

(38) Sudant, G.; Baudrin, E.; Dunn, B.; Tarascon, J.-M. Synthesis and Electrochemical Properties of Vanadium Oxide Aerogels Prepared by a Freeze-Drying Process. *J. Electrochem. Soc.* **2004**, *151* (5), A666. https://doi.org/10.1149/1.1687427.

(39) Hekmatfar, M.; Kazzazi, A.; Eshetu, G. G.; Hasa, I.; Passerini, S. Understanding the Electrode/Electrolyte Interface Layer on the Li-Rich Nickel Manganese Cobalt Layered Oxide Cathode by XPS. *ACS Appl. Mater. Interfaces* **2019**, *11* (46), 43166–43179. https://doi.org/10.1021/acsami.9b14389.

(40) Fan, X.; Chen, L.; Borodin, O.; Ji, X.; Chen, J.; Hou, S.; Deng, T.; Zheng, J.; Yang, C.; Liou, S. C.; Amine, K.; Xu, K.; Wang, C. S. Non-Flammable Electrolyte Enables Li-Metal Batteries with Aggressive Cathode Chemistries. *Nat. Nanotechnol.* **2018**, *13* (8). https://doi.org/10.1038/s41565-018-0183-2.

(41) Zarrabeitia, M.; Gomes Chagas, L.; Kuenzel, M.; Gonzalo, E.; Rojo, T.; Passerini, S.;

Muñoz-Márquez, M. Á. Toward Stable Electrode/Electrolyte Interface of P2-Layered Oxide for Rechargeable Na-Ion Batteries. *ACS Appl. Mater. Interfaces* **2019**, *11* (32), 28885–28893. https://doi.org/10.1021/acsami.9b07963.

(42)   Levi, M. D.; Lu, Z.; Aurbach, D. Application of Finite-Diffusion Models for the Interpretation of Chronoamperometric and Electrochemical Impedance Responses of Thin Lithium Insertion V2O5 Electrodes. *Solid State Ionics* **2001**. https://doi.org/10.1016/S0167-2738(01)00819-0.

(43)   Boukamp, B. A. A NONLINEAR LEAST SQUARES FIT PROCEDURE FOR ANALYSIS OF. **1986**, *20*, 31–44.
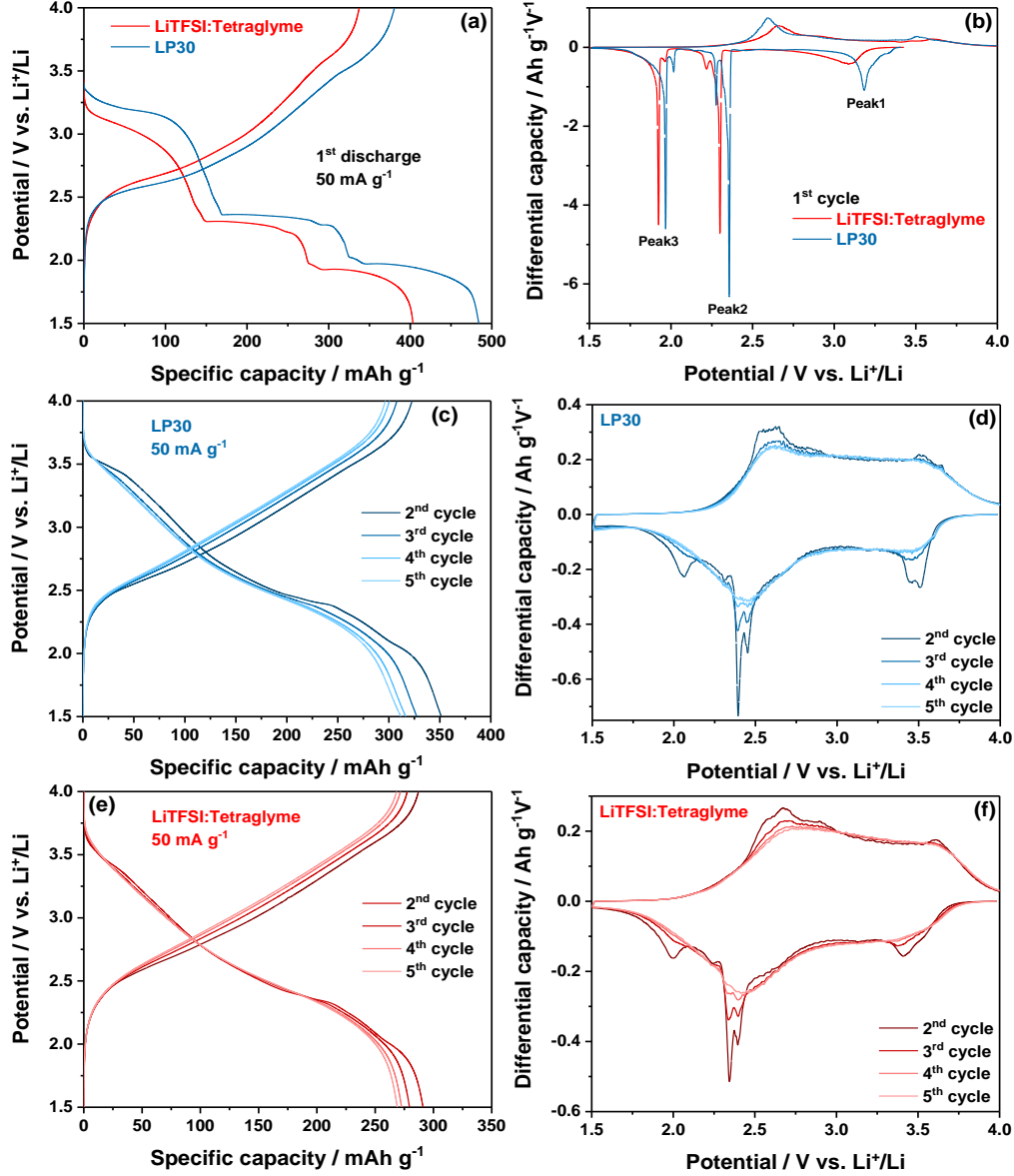
Figure 1. First cycle (a) charge-discharge profiles and (b) corresponding differential capacity profiles of the Li/V_2O_5 cells using LP30 and LiTFSI:Tetraglyme electrolytes. Panels (c) and (e) show the charge-discharge profiles of Li/V_2O_5 cells during the 2nd – 5th cycles using, respectively, the LP30 and LiTFSI:Tetraglyme electrolytes. The calculated differential capacity plots in the 2nd – 5th cycles of the Li/V_2O_5 cells using (d) LP30 and (f) LiTFSI:Tetraglyme electrolytes. Galvanostatic cycling test performed at 50 mA g^{-1} and 20°C.
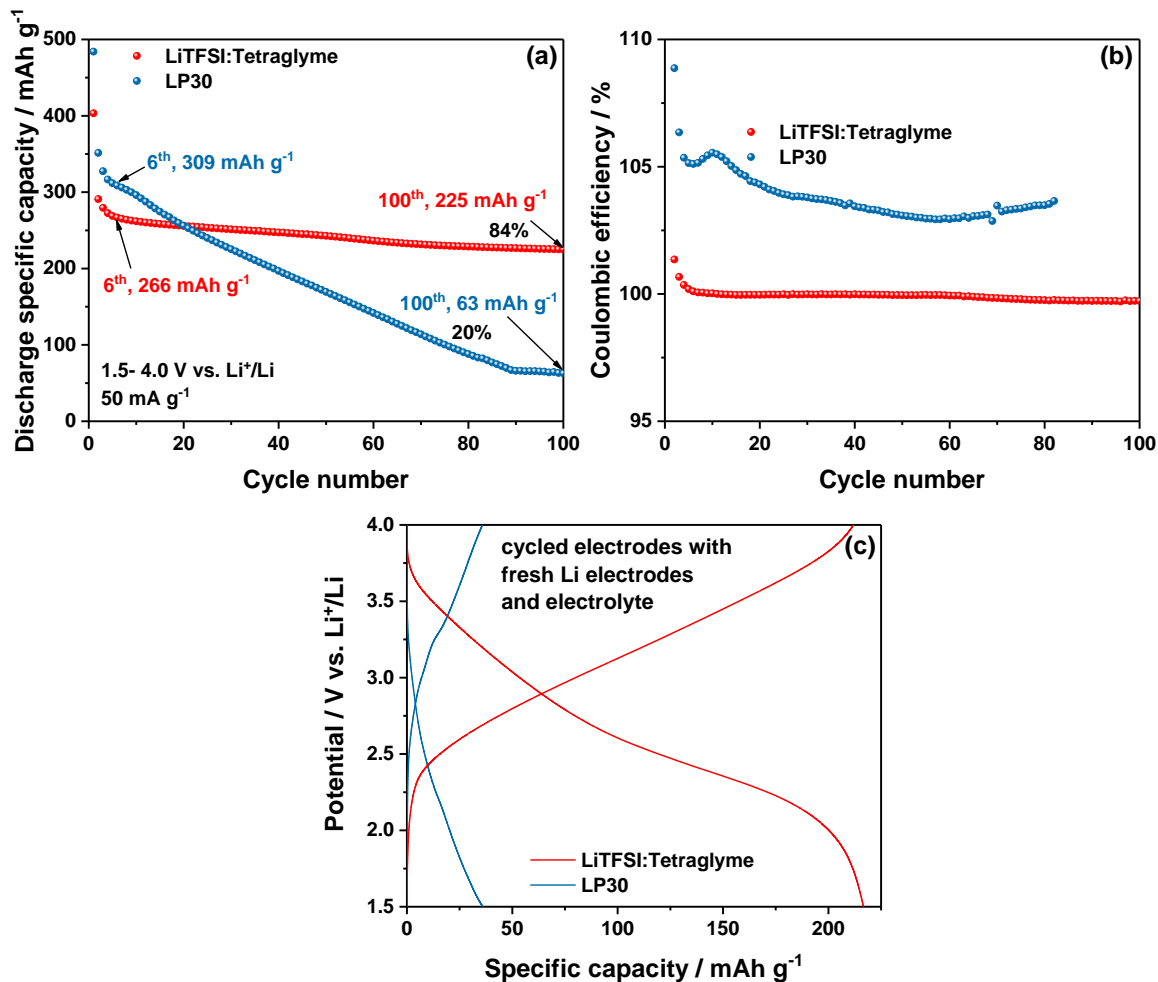
Figure 2. Evolution of (a) discharge specific capacity and (b) Coulombic efficiency of the Li/V$_2$O$_5$ cells employing different electrolytes (see legends) upon cycling ability tests at 50 mA g^{-1} within 1.5-4.0 V vs. Li$^+$/Li. (c) The charge-discharge curve of the Li/V$_2$O$_5$ cells using cycled V$_2$O$_5$ electrodes and refreshed Li electrodes and electrolytes at 50 mA g^{-1}.
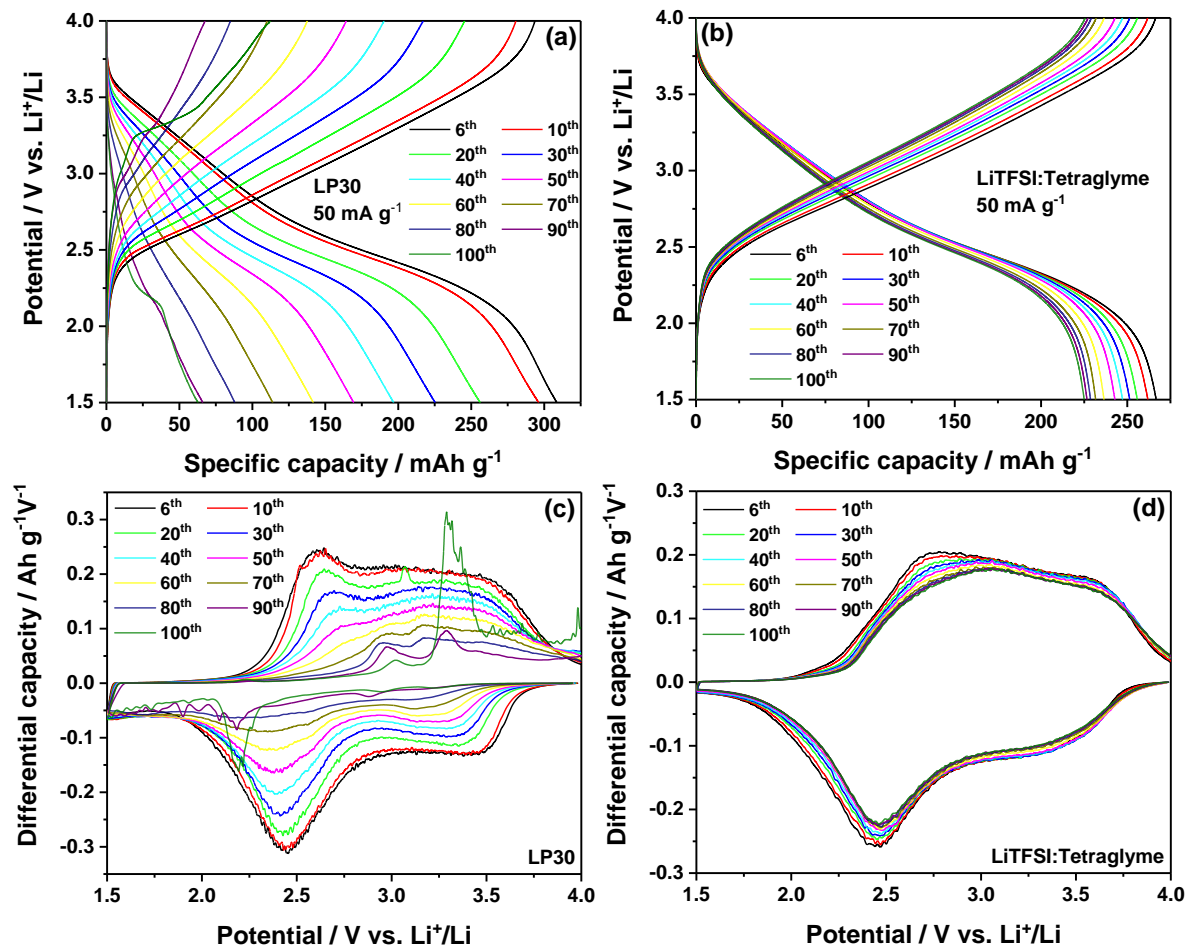
Figure 3. Selected charge-discharge profiles of the Li/V$_2$O$_5$ cells using (a) LP30 and (b) LiTFSI:Tetraglyme electrolytes, respectively. The calculated differential capacity plots of the Li/V$_2$O$_5$ cells using (c) LP30 and (d) LiTFSI:Tetraglyme electrolyte, respectively.
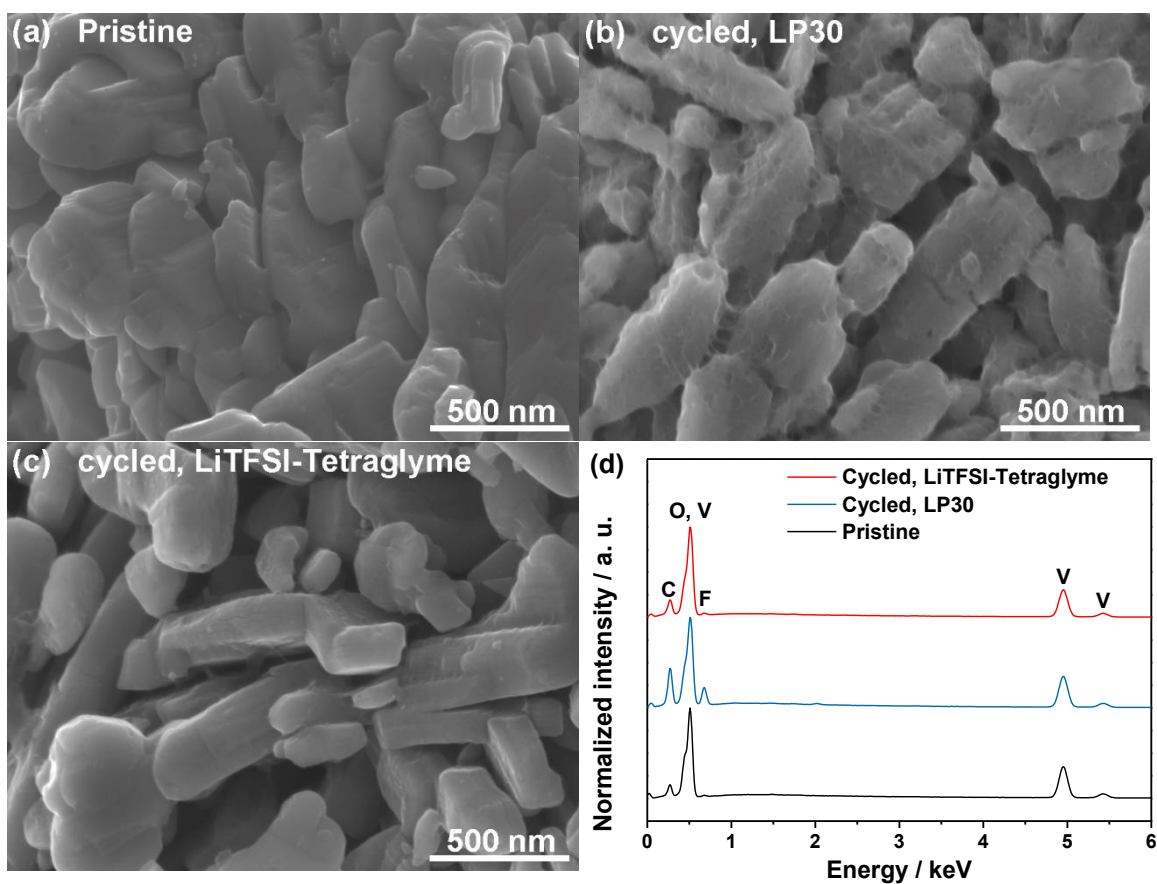
Figure 4. SEM images of V_2O_5 in (a) pristine electrode, and electrodes cycled in (b) LP30 and (c) LiTFSI:Tetraglyme electrolytes, and (d) corresponding EDX spectra.
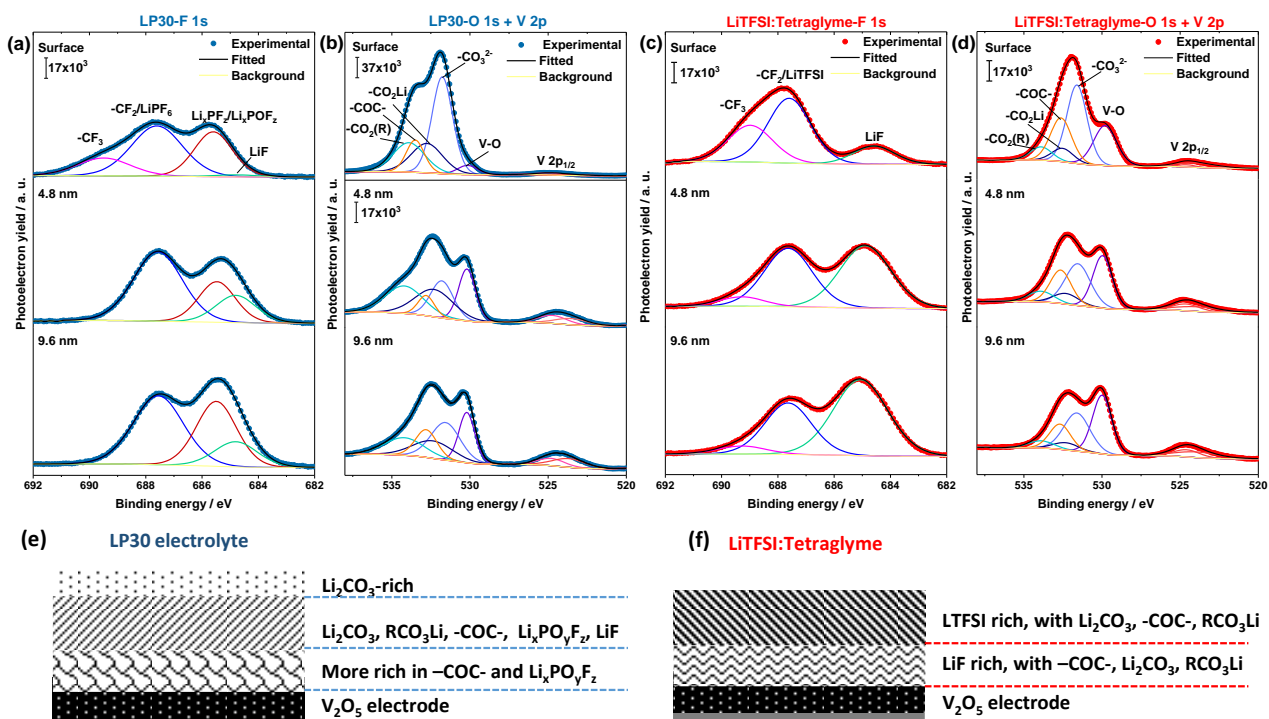
Figure 5. F 1s and O 1s + V 2p photoelectron spectra at different depths (surface, 4.8 and 9.6 nm) of the V_2O_5 electrode after 100 charge-discharge cycles in (a,b) LP30 and (c,d) LiTFSI:Tetraglyme electrolytes, respectively. The schematic of the CEIs formed in (e) LP30 and (f) LiTFSI:Tetraglyme electrolytes.
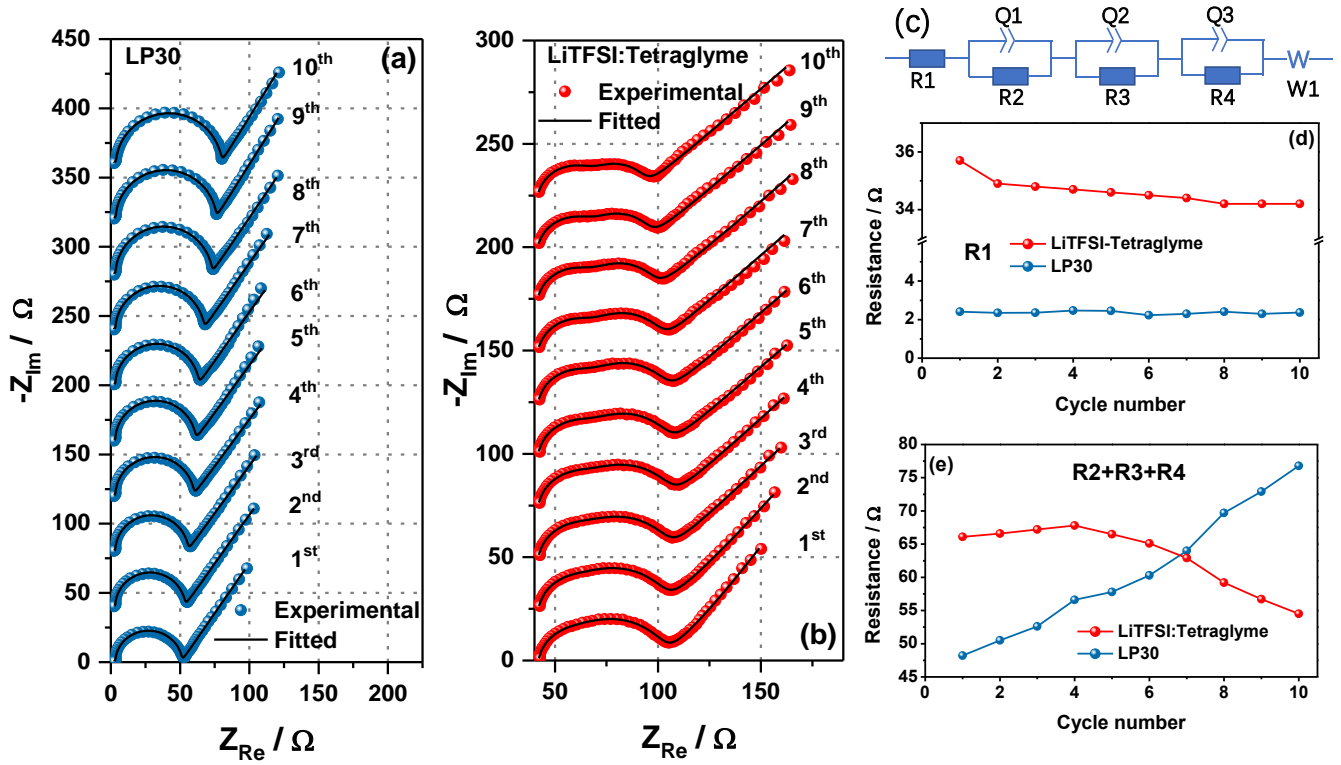
Figure 6. The Nyquist plots of the V_2O_5 electrode in the initial 10 cycles in (a) LP30 and (b) LiTFSI:Tetraglyme electrolytes. (c) The equivalent electrical circuit used for fitting. The resistance evolution of (d) R1 and (e) R2+R3+R4 upon the initial 10 cycles.

ToC graphic